2nd4

NASA TECHNICAL MEMORANDUM

NASA TM X-71502

NASA TM X- 71502

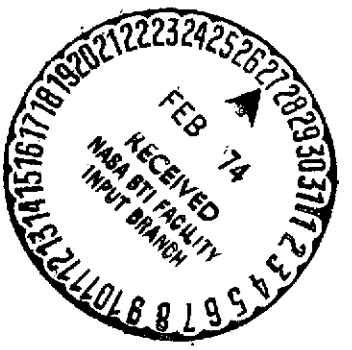

RATIONAL FUNCTION REPRESENTATION OF FLAP NOISE SPECTRA INCLUDING CORRECTION FOR REFLECTION EFFECTS

by J. H. Miles
Lewis Research Center
Cleveland, Ohio 44135

TECHNICAL PAPER proposed for presentation at Twelfth Aerospace Sciences Meeting sponsored by the American Institute of Aeronautics and Astronautics Washington, D.C., January 30-February 1, 1974

RATIONAL FUNCTION REPRESENTATION OF FLAP NOISE SPECTRA INCLUDING CORRECTION FOR REFLECTION EFFECTS

by J. H. Miles

Lewis Research Center
National Aeronautics and Space Administration
Cleveland, Ohio

ABSTRACT

A rational function is presented for the acoustic spectra generated by deflection of engine exhaust jets for under-the-wing and over-the-wing versions of externally blown flaps. The functional representation is intended to provide a means for compact storage of data and for data analysis. The expressions are based on Fourier transform functions for the Strouhal normalized pressure spectral density, and on a correction for reflection effects based on the N-independent-source model of P. Thomas extended by use of a reflected ray transfer function. Curve fit comparisons are presented for blown flap data taken from turbofan engine tests and from large scale cold-flow model tests. Application of the rational function to scrubbing noise theory is also indicated.

E-7869

INTRODUCTION

Future short takeoff and landing (STOL) aircraft will undoubtedly be required to meet stringent noise level regulations. Thus, noise is one of the primary factors in the selection of a STOL propulsion-lift system. One candidate source of propulsive-lift is the externally blown flap (EBF) system. Propulsive lift is generated by downward deflection of engine exhaust jets in either the under-the-wing or the over-the-wing version of EBF. Each EBF STOL concept introduces noise sources not present in conventional takeoff and landing (CTOL) airplanes which cause an increase in noise. These EBF STOL propulsive lift concepts are being investigated by scale model tests (refs. 1 to 8), and full scale engine tests (refs. 9 and 10). Concurrently, theoretical and experimental studies are being conducted on various noise source mechanisms (refs. 11 to 14), and empirical prediction methods are being devised (ref. 15).

The objective of this paper is to determine a rational function representation of flap noise spectra that is useful (1) as an empirical equation to fit EBF STOL spectral data, and (2) as a function that can be related to certain noise-source mechanisms. The rational function representation is intended to serve as a link between experimental EBF spectral data and theoretical explanations, and to provide a mathematical expression for EBF noise spectra that can become part of an empirical prediction method.

Many noise source mechanisms may contribute to the overall noise of an EBF system. These include: (1) leading edge noise caused by incident turbulence; (2) scrubbing noise generated in the turbulent boundary layer produced by the jet mixing region and convected along the wing or flap; (3) separated flow noise; (4) trailing-edge noise caused by vortex shedding of eddies from the deflected flap; (5) jet mixing noise from the distorted deflected exhaust jet; and (6) engine internal and turbomachinery noise. Each of these sources may dominate at some angle depending on the specific jet exhaust velocity and EBF STOL configuration.

The noise source mechanism receiving most emphasis is the one to which scrubbing noise is attributed (refs. 16 through 25). In spite of many advances in understanding this and other noise sources, procedures for calculating noise from EBF STOL airplanes starting with basic aeroacoustic mechanisms are not available currently. Hence, present design studies depend on model and full scale tests and on empirical relations determined from these tests.

For design studies, one of the most important aspects of the measured noise is the third-octave sound pressure level spectrum designated in this report by SPL. It is used to compute the perceived noise level (PNL) and the effective perceived noise level (EPNL), which are the present criteria used to judge the effect of an aircraft on the community noise level.

This report describes an empirical rational function that can be used to represent the SPL data. The function provides a representation for broadband SPL spectra. With the representation described, sound spectra can be stored in a computer in a compact form and comparison of large amounts of data from different experiments is facilitated. The representation can also be used to extrapolate data to untested conditions, which is useful in making estimates of PNL, EPNL, and footprint calculations. In functional form, new relations or physical insights into source mechanisms may more easily become apparent. In fact, the empirical functional representation is related herein to a theoretical description of scrubbing noise, and thus provides a reason for the observed similarity of EBF data. In achieving this functional representation, corrections for acoustic reflections in ground test data are taken into account.

The paper will present the development of equations representing the spectra. A basic equation is given in terms of the spectral density of a real random process. This equation will be related to scrubbing noise theory. Next, a simplified equation that represents the spectra will be given. Equations for corrections for reflection and atmospheric effects will also be included. The complete calculation method will then be discussed, and finally, results from EBF data taken from turbofan engine tests and cold flow tests of under-the-wing and over-the-wing test models will be given.

ANALYSIS

Approach

The approach taken to represent flap noise spectra is based upon finding a function of Strouhal number, $\phi(\Omega)$, such that the third-octave sound pressure level (SPL) can be fitted by

$$SPL(\ell) = 10 \log_{10}\left\{\left[10^{OASPL/10}\right]\left[\Delta f_c(\ell)\,\frac{D_e}{V_e}\right]\phi(\Omega)\right\} \tag{1}$$

where

$$OASPL = 10 \log_{10}\left[\Sigma_\ell\ 10^{SPL(\ell)/10}\right] \tag{2}$$

D_e is an effective diameter (refs. 7, 8, and 15)

V_e is an effective velocity (refs. 7, 8, and 15)

and

ℓ refers to the ℓ^{th} third octave frequency band

(All symbols are defined in the symbol list.) Specifically,

$$\Omega = j2\pi\left(f_c\,\frac{D_e}{V_e}\right) = j2\pi St \tag{3}$$

The requirements on the function $\phi(\Omega)$ are:

(1) It should be tailored for applicability to large Strouhal numbers. Curve fits that are accurate at large Strouhal numbers are necessary, since externally blown flap engines are likely to have large effective diameters and low exhaust velocities.

(2) It should be consistent with theoretical considerations.

(3) It should depend on as few mathematical coefficients and operations as possible since this will reduce computer calculation time.

(4) It should be applicable to a wide range of system configurations (e.g., single or coannular nozzles, mixer nozzles, over-the-wing, and under-the-wing, etc.).

From equation (1),

$$10 \log_{10}\{\phi(\Omega)\} = SPL(\ell) - OASPL - 10 \log_{10}\left[\Delta f_c(\ell)\,\frac{D_e}{V_e}\right] \tag{4a}$$

The quantity represented by equation (4a) is the Strouhal normalized mean-square pressure spectral density level per unit Strouhal number. In this paper expression (4a) will be referred to as the PSD^+ function. PSD^+ which is a function of Strouhal number is calculated from SPL data free of atmospheric absorption and reflection effects (lossless data). It has been shown that spectral data taken over a range of exhaust velocities for numerous engine-over-the-wing and engine-under-the-wing externally blown flap configurations correlate when plotted in terms of the PSD^+ function (e.g., refs. 3 and 4). Thus,

$$PSD^+ = 10 \log_{10}[\phi(\Omega)] \tag{4b}$$

where $\phi(\Omega)$ is seen to be the Strouhal normalized mean square pressure spectral density per unit Strouhal number.

Since the acoustic noise generation is basically a random process, a function form for $\phi(\Omega)$ will be selected such that it represents the power spectral density of a real random process. The expression will also be capable of fitting a wide range of PSD^+ data. This basic functional form will be related to a theoretical description of scrubbing noise. Next, the basic expression will be simplified by removing certain factors. The simplified expression will also fit the PSD^+ curve, but having fewer terms it can be evaluated faster in a computer calculation.

Finally, the equations necessary to relate the calculated lossless PSD^+ curve to SPL data affected by ground reflections and atmospheric attenuation will be stated. The basis for the correction is discussed, and some examples of the ground reflection effect are presented.

Spectral Density Function

Basic function. - The mathematical criteria that $\phi(\Omega)$ must satisfy to represent a power spectral density is that it must not be negative and must be integrable. However, to represent the power spectral density of a real random process, $\phi(\Omega)$ must also be an even function of Strouhal number. A basic function having these properties can be formulated from the reciprocal of the Fourier transform of a "damped cosine oscillation." Explicitly, the function is

$$\sigma(\Omega,c) = \frac{(\Omega - c)(\Omega - c^*)}{\Omega + \sqrt{cc^*}} \tag{5}$$

where c represents a complex number and the asterisk (*) indicates the conjugate relation.

The function $\sigma(\Omega,c)$ defines a curve of σ for a given value of c. Since the desired expression for $\phi(\Omega)$ involves the logarithmic addition of a number of individual $\sigma(\Omega,c)$ curves (to fit observed PSD^+ variation),

the general expression for a real random process, $\phi_{Real}(\Omega)$, can be expressed as the ratio of the products of these terms,

$$\phi_{Real}(\Omega) = \left| \frac{a_o \prod_{i=1}^{M_a} \sigma(\Omega, a_i)}{\prod_{k=1}^{N_b} \sigma(\Omega, b_k)} \right|^2 \tag{6}$$

a_o is a normalization constant; the complex numbers a_i and b_k have negative real values and positive or zero imaginary values; and M_a is less than N_b. The individual curves comprising the total function $\phi_{Real}(\Omega)$ are referred to as Strouhal response functions. The unknown in equation (6) is the number of response functions and their value (a_i and b_k terms) required to properly fit a given data variation.

Application to scrubbing noise theory. - Equation (6) can be used to yield inputs to a theoretical description of scrubbing noise. Starting from Curle's extension of Lighthill's theory to surfaces (ref. 16), it is possible to show that dipole broadband noise is radiated from a rigid surface adjacent to a turbulent boundary layer. The noise produced is referred to as scrubbing noise. The mean square pressure per unit Strouhal number from references 24 and 25 would correspond to

$$\phi(\Omega) = \frac{|\Omega|^2 \int_S \psi(\Omega) A_c(\Omega) dS(\vec{x})}{(2\pi)^2 \int_0^\infty St^2 \int_S \psi(\Omega) A_c(\Omega) dS(\vec{x}) dSt} \tag{7}$$

in the notation of this paper, where $S(\vec{x})$ represents the surface immersed in a flow, $\psi(\Omega)$ is the spectrum of the pseudo-sound or fluctuating surface pressure, and $A_c(\Omega)$ is the correlation area over which the normalized cross spectral density of the normal stress is unity.

Some attempts have been made to define equations for $\psi(\Omega)$ and for $A_c(\Omega)$ based on experimental data for surfaces other than flaps (refs. 24 and 25). The necessary measurements do not exist specifically for flap noise sources. However, empirical representations of the $\psi(\Omega)$ and $A_c(\Omega)$ functions for flap noise have been made based on experimental data of similar phenomena. In reference 14, Fink approximated the correlation area (in the notation of this paper) by

$$A_c(\Omega) \cong \left| \frac{2\pi}{(\Omega - \alpha_o)} \right|^2 \tag{8a}$$

and the static pressure fluctuation spectrum was approximated by

$$\psi(\Omega) \cong \left| \frac{2\pi(\Omega - \alpha_o)}{(\Omega - b_1)(\Omega - b_2)} \right|^2 \tag{8b}$$

where

$$b_1 = \pi St_o\sqrt{2}\ (-1 - j)$$

$$b_2 = \pi St_o\sqrt{2}\ (-1 + j)$$

Expressions for these two functions can also be postulated from equation (6) as follows:

$$A_c(\Omega) = \left| \frac{\prod_{i=1}^{M_a} \sigma(\Omega, a_i)}{\prod_{m=1}^{K_d} \sigma(\Omega, d_m)} \right|^2 \tag{9a}$$

and

$$\psi(\Omega) = \left| \frac{\prod_{m=1}^{K_d} \sigma(\Omega, d_m)}{\prod_{k=1}^{N_b} \sigma(\Omega, b_k)} \right|^2 \tag{9b}$$

where $M_a < K_d < N_b$ and d_m has a negative real part and a zero or positive imaginary part.

The expressions of equation (9) are more general and provide greater flexibility than the expressions of equation (8). The greater number of coefficients in equation (9) compared to equation (8) increase the potential ability of the functions to fit experimentally based $A_c(\Omega)$ and $\psi(\Omega)$ functions and should also be more useful in fitting PSD data.

Simplified function. - Equation (6) is the power spectral density of a real random process. A modification of equation (6) that yields a simpler expression which is equally suitable for representing PSD$^+$ data will be discussed next. However, while the new equation can be used to satisfactorily fit a spectral density it does not represent a power spectral density of a real random process.

The modification consists of dropping the term $(\Omega - c^*)/(\Omega + \sqrt{cc^*})$ from equation (5). The equation for the calculated lossless PSD^+ then can be written as

$$PSD^+_{cal} = 10 \log_{10} \left| \frac{a_o \prod_{i=1}^{M_a} (\Omega - a_i)}{\prod_{k=1}^{N_b} (\Omega - b_k)} \right|^2 \qquad (10)$$

where all symbols are the same as in equation (6).

Reflection Correction

Acoustic reflections cause problems, since in some experiments reflections distort the true sound spectrum and lead to incorrect spectral shapes with frequent overestimation of the overall sound pressure level (OASPL). The reflection correction developed herein is based on a mathematical model. Reflection model parameters are adjusted simultaneously with the functional representation parameters of equation (10) by the computer program. The calculated SPL depends on both sets of parameters. In situations where the acoustic reflection model parameters are unknown, the functional representation plays a vital part in correcting reflection effects. A description of the reflection model and some examples are provided herein.

The measured sound pressure level, without atmospheric attenuation obtained by including reflection effects with the lossless value of SPL^+ is given by

$$SPL(f_c) = SPL^+(f_c) + 10 \log_{10} |T(f_c)|^2 \qquad (11)$$

where $|T(f_c)|^2$ is the reflectance and $SPL^+(f_c)$ (eq. (1)) is the sound pressure level without atmospheric attenuation and ground reflection.

In arriving at equation (11) the model assumes the noise source is distributed over a region and represents this by rays from N independent sources. This assumption was used by P. Thomas (ref. 26) to study acoustic interference of the noise produced by a single jet due to reflections from a plane. An alternative treatment for a distributed source using the wave equation is given in reference 27. The ground reflection effect on a single point noise source has been treated in references 28 to 31.

The working hypothesis will be that the noise can be treated as if it were from a vertical arrangement of N independent sources of equal

strength at the trailing edge of the last flap. This model permits one to consider a microphone at a particular angle to be receiving reflections from the wing, flap and ground surfaces, resulting in an angle-dependent interference effect.

The sound reaching the microphone is assumed to consist of the sound that travels the direct path, going a distance s_1, and the sound that travels a reflected path going a distance s_2 (fig. 1). Since the reflected path is longer than the direct path, the reflected sound reaches the microphone after a time delay τ where $\tau = (s_2 - s_1)/c_o$ relative to the direct sound that left at the same time. Thus if the direct wave reaching the microphone was emitted at a time t, the reflected wave reaching the microphone at the same time is due to one emitted at a time $t - \tau$.

Many point sources are assumed to be causing the sound and each source is assumed to produce reflections from wing, flap, and ground surfaces. This causes many reflection paths. The amplitude of the reflected sound is changed by these multiple reflections before the signal reaches the microphone. The modification to the reflected pressure signal will be assumed to be related to the direct ray by a convolution of the reflecting surfaces' impulse response with the direct pressure signal:

$$p'(t) \triangleq \int_0^\infty g(\tau)p(t - \tau)d\tau \tag{12}$$

The Laplace transform of the reflecting surface impulse response $g(\tau)$ is the reflected ray transfer function $G(s)$. This complex reflected ray transfer function can also be written in terms of its phase δ and amplitude $|Q|$. Thus,

$$G(s) = |Q(s)|e^{j\delta(s)} \triangleq \int_0^\infty g(\tau)e^{-\tau s}\, d\tau \tag{13}$$

The source, flap, and microphone geometry with respect to the ground plane is shown schematically in figure 1. Each of the N-independent sources will be assumed to produce a direct ray that travels a distance s_1. All the sources will be assumed to be at a fixed distance r from all the microphones. For the n^{th} source at a height $h_s(n)$

$$s_1(n) = \left\{r^2 + [h_s(n) - h_o]^2\right\}^{1/2}$$

The reflected ray path distance for the n^{th} source is

$$s_2(n) = \left\{r^2 + [h_s(n) + h_o]^2\right\}^{1/2}$$

The observed relative pressure at a distance r will be given by the sum of the pressure signals traveling directly from the N sources and the reflected pressure signals which are delayed by a time delay τ_n relative to the direct signals and reduced by a divisor, z, proportional to the ratio of the travel distance of the reflected pressure signal to the direct pressure signal. The variation of the heights of the source, relative to the radial distance is assumed small; thus the mean value of the ratio of the reflected signal travel distance to the direct signal travel distance will be used.

The resulting mean-square pressure spectrum density at the microphone is found by a two-step procedure. First the auto-correlation of the signal is found. Then the Laplace transform of the auto-correlation is taken. This two-step procedure is used to obtain the frequency response since the noise will be assumed to be produced by a stationary independent random process.

The spectrum without attenuation is assumed to be the sum of the spectra of the N sources. These sources are also assumed to be of equal strength. If the source spectrum, $|Q(s)|$ and $\delta(s)$ are assumed to be constant over any third-octave band, the third-octave spectrum (neglecting atmospheric attenuation) measured at the microphone is given by equation (11) where the reflectance, $|T(f_c)|^2$, is given by

$$|T(f_c)|^2 = 1 + \frac{|Q(f_c)|^2}{z^2} + \frac{2}{N}\frac{|Q(f_c)|}{z}\sum_{n=1}^{N}\cos[2\pi f_c \tau_n - \delta(f_c)]\,\frac{\sin(\pi\,\Delta f_c \tau_n)}{\pi\,\Delta f_c \tau_n} \tag{14}$$

For use in the determination of $|T(f_c)|^2$ by a computer, the reflected ray transfer function G(s) will be assumed to be independent of frequency. Hence in equation (14), $|Q(f_c)|$ and $\delta(f_c)$ will be replaced by the constants $|Q|$ and δ.

Typical reflectances for a low and high level of $|Q|$ are shown in figures 2 and 3. Figure 2 applies to the test configuration at the cold flow model test site (ref. 4) and figure 3 applies to the test configuration at the EBF test site (refs. 9 and 10). Table I contains the values of the constants used in the reflectance calculations. The effect of low $|Q|$ values is to minimize the magnitude of the cancellations and reinforcements.

CALCULATION METHOD

The complete equation used to represent the SPL at a microphone location for a given configuration is based on equations (1), (4), (10), (11), and (14),

$$SPL_{cal} = 10 \log_{10}\left\{\left[10^{OASPL_p^+/10}\,\Delta f_c\,\frac{D_e}{V_e}\right]\times\left[\left|\frac{a_o\prod_{i=1}^{M_a}(\Omega - a_i)}{\prod_{k=1}^{N_b}(\Omega - b_k)}\right|^2\right]\times\left[1 + \frac{|Q|^2}{Z^2} + \frac{2}{Z}\frac{|Q|}{N}\sum_{n=1}^{N}\cos(2\pi f_c\tau_n - \delta)\,\frac{\sin(\pi\,\Delta f_c\tau_n)}{\pi\,\Delta f_c\tau_n}\right]\right\} + A_T(f_c,r) \tag{15}$$

where $A_T(f_c,r)$ is the atmospheric attenuation. The atmospheric attenuation was computed by the method of reference 32.

A computer program is used to adjust the parameters $OASPL_p^+$, a_o, a_i; $i = 1, \ldots, M_a$, b_k; $k = 1, \ldots, N_b$, $|Q|$ and δ. A diagram of the method is shown in figure 4. The parameters are adjusted to minimize the total "cost," C_T, consisting of the sum of the squares of the differences between the measured and calculated SPL values, C_e, and a penalty cost C_p (refs. 33 and 34) due to selection of parameters that violate the parameter constraints previously mentioned. (See eq. (2) for $OASPL_p^+$ constraint and eq. (6) for a_i and b_k constraint.) The total cost function is nonlinear. The problem of minimizing the nonlinear cost function was solved by search techniques. These techniques consist of systematic procedures for varying the cost function parameters until a minimum value of the cost function is found. The basic methods available are discussed in references 33 and 34. To provide flexibility in the choice of M_a and N_b and due to the presence of parameter constraints, a search technique which does not require evaluation of derivatives was chosen. The search technique was that of Powell (ref. 35). The computer program used was adapted from reference 36. The optimization procedure was previously applied successfully to a similar identification problem in reference 37.

The input information for the method consists first of the constants required for the reflection model. These consist of the following: the number of sources, N, which was selected to be 5; the mean value of the ratio of the distance the reflected ray travels to the distance the direct ray travels, z; and the time delay, τ_n associated with each of the five sources. Second, the constants M_a and N_b for the PSD_{cal}^+ model are needed. For the data considered N_b was selected to be 3 and M_a

was selected to be 1. Last, initial values of the parameters to be varied ($OASPL_p^+$, a_o, $|Q|$, δ, a_1, b_1, b_2, b_3) are necessary.

RESULTS

The calculation method based on the rational PSD^+ function with reflection corrections was applied to several sets of measured data to illustrate the comparisons obtained for the PSD^+ function and for both measured and corrected SPL spectra. Also included are examples of OASPL variations with exhaust velocity and PSD^+ functions over a range of microphone angles.

Basic PSD^+ Function

Several sets of lossless blown flap data are available for determining fits by the PSD^+ function based on the formulation for a real random process given by equation (6). Data correlations over a range of exhaust velocities in terms of lossless spectral density versus Strouhal number are available in reference 3 for a cold flow test of an under-the-wing externally blown flap configuration. Comparable Strouhal correlations for a cold flow over-the-wing configuration with attached flap flow (powered lift) and with unattached flow (conventional lift) are presented in reference 4. Calculated values of PSD^+ for these data were obtained from iterative calculations of equations (6) and (4b) in conjunction with the measured values of PSD^+. A total of nine parameters were used in the calculation. The parameter values corresponding to the best fit of the data are given in table II.

Figure 5 shows a comparison of the data and the curve fit for PSD^+ for the under-the-wing model of a flap setting of 30^o - 60^o for the 85^o microphone angle position. Figure 6 shows a comparable comparison at a microphone angle of 100^o above an over-the-wing model with attached flow at a flap setting of 10^o - 20^o. The comparison for the unattached flow version of the over-the-wing model with flap settings of 10^o - 20^o and 30^o - 60^o are shown in figure 7. In all cases, the calculated curve fits are in very good agreement with the data over the entire Strouhal number range. Thus, equation (6) should be applicable to data from many different types of blown flap configurations.

Simplified PSD Function

The simplified PSD^+ function of equation (10) was also used to fit the data shown in figures 5 to 7. The nine parameters obtained are shown in table III in terms of the complex constants needed for the fit. In all cases, the curve fit to the data was very nearly as good as for the basic function of equation (6). An example of the comparison is given in figure 8 which shows the calculated PSD^+ values for the basic (eq. (6)) and simplified (eq. (10)) functions as obtained for the fit of the data

of figure 6. On the basis of the close correspondence of the two results, it was concluded that the simplified version of the PSD^+ function given by equation (10) is completely adequate for routine calculation purposes.

Number of Parameters

The curve fits used in fitting the data shown in figures 5 to 7 were based on using $M_a = 1$ and $N_b = 3$, which results in nine parameters in equations (6) and (10). Figure 9 is a plot of the individual Strouhal response functions $F(a_1)$, $F(b_1)$, $F(b_2)$, $F(b_3)$ corresponding to a_1, b_1, b_2, and b_3 that make up the simplified PSD^+ functions of figure 8. The b_3 curve is seen not to contribute to the final curve form. In fact, if the magnitude of b_i (i = 1, 2, or 3) is larger than 60 and the maximum Strouhal number of interest is less than 50, the value of $F(b_i)$ is nearly zero and $\sigma(\Omega,b_i)$ is nearly constant and has a value of $\sqrt{b_i b_i^*}$. Therefore, b_i can be eliminated and the number of parameters required can be reduced from nine to seven. Tables II and III show that for each of the four curves, the magnitude of one of the b_i is larger than 60. Consequently a seven-parameter formulation of equation (6) or (10) should be adequate for many calculations.

Application to Scrubbing Noise Theory

Two sets of functions were presented earlier for the correlation area $A_c(\Omega)$ and the static pressure fluctuation spectrum $\psi(\Omega)$ for equation (7) describing flap surface scrubbing noise. One functional form of $\phi(\Omega)$ based on using equation (8a) for $A_c(\Omega)$ and equation (8b) for $\psi(\Omega)$ with $St_o = 0.3$ was developed by Fink (ref. 14). The particular form of the denominator parameters selected by Fink results in a $\phi(\Omega)$ function that depends on only a single constant, St_o; however, in the notation of this paper, this functional form consists of three parameters. In arriving at this total the normalization constant, a_0 is counted as one parameter of $\phi(\Omega)$. Also the functional form of $\phi(\Omega)$ will be said to have two parameters in the denominator. This is done since a complex constant and its complex conjugate are counted only once and equation (8) indicates the two parameters (b_1 and b_2) in the denominator of $\phi(\Omega)$ are conjugate complex constants.

The other functional form based on equations 9(a) for $A_c(\Omega)$ and 9(b) for $\psi(\Omega)$ is the one developed in this paper. This functional form, as has been previously discussed, was found to give a good fit to the data with $M_a = 1$ and $N_b = 2$, to yield a total of seven parameters. Thus, the major characteristic of equation (9) compared to equation (8) is the addition of two parameters to the numerator and two parameters to the denominator with freedom to select the six best parameters for the numerator and denominator.

In figure 10 the ability of two different functional forms of $\phi(\Omega)$

to fit the data shown in figure 5 is compared. Each PSD^+ curve shown in figure 10 is calculated from equation (4) which relates the PSD^+ curve to the $\phi_{Real}(\Omega)$ function and from equation (7) which relates the $\phi_{Real}(\Omega)$ function to the correlation area, $A_c(\Omega)$, and the static pressure fluctuation spectrum $\psi(\Omega)$. The three-parameter functional form of $\phi(\Omega)$ derived by Fink with St_o set equal to 0.3 was found to be in general agreement with the data of figure 5 but overestimates the PSD^+ at large Strouhal numbers as mentioned by Fink (ref. 14). This can be seen in figure 10 where the seven-parameter curve that provides an exact fit to the data of figure 5 is compared with three-parameter curve fit. Thus, the greater number of coefficients in the functional form of $\phi_{Real}(\Omega)$ developed in this paper and the use of the computer to find the best parameters provides an excellent curve fit to PSD^+ data.

Application to Measured Data

Cold flow model. - Measured and calculated values are compared in figure 11 for a number of calculated quantities for the case of data from an over-the-wing model (ref. 4) with two wing flaps and attached flap flow (powered lift configuration). The test configuration is for cold flow with a circular nozzle and a flap setting of $10^o - 20^o$.

Figure 11(a) shows the measured third-octave sound pressure level spectrum. The data were taken at an exhaust velocity of 253 m/sec (830 ft/sec) and a microphone angle of 100^o from the inlet. The cancellations denoted by C_1, C_2, C_3 and the reinforcements denoted by R_2, R_3, R_4 are due to reflection effects. Figure 11(b) shows the measured sound pressure level, SPL_M, the calculated SPL including effects of atmospheric absorption and reflections, SPL_{cal}, and the calculated lossless sound pressure level, SPL^+_{cal}. The reflectance used to account for the reflection effect is that shown in figure 2(b). Comparison between measured (SPL_M) and calculated (SPL_{cal}) spectra indicates that SPL_{cal} gives a good fit to the data.

Figure 12 illustrates the fit between calculated values of lossless spectral density, PSD^+_{cal}, and the PSD^+ spectrum obtained from the measured SPL by using the calculated reflectance shown in figure 2(b) and a calculated atmospheric attenuation. This calculated PSD based on the measured SPL data is denoted as PSD^+_M. The close proximity of the least square curve fit, PSD^+_{cal}, to the PSD^+_M calculated points is apparent.

Full-scale engine configuration. - Another example of the application of the method is given for a set of data from the tests of reference 9 for a full-scale EBF system with a three-flap wing and a turbofan engine with a coannular nozzle. The test condition is for a takeoff flap setting of 0^o-20^o-40^o, an effective exhaust velocity of 242.3 m/sec (795 ft/sec) (maximum power), and a microphone angle of 80^o from the inlet. Figure 13(a) shows the measured third-octave SPL spectrum for the test condition. Reflection effects are indicated by the first cancellation denoted by C_1 and by the second reinforcement denoted by R_2. The

turbofan engine in this program was highly noise suppressed (ref. 10) with much of the fan discrete tone noise removed. However, because some residual fan tone noise may be present at frequencies above 4000 hertz for the maximum power operating test condition only data from 50 to 3150 hertz were analyzed herein.

The calculated spectrum for lossless sound pressure level, SPL^+, is shown in figure 13(b). Also shown are calculated values of SPL including reflection and atmospheric attenuation effects, SPL_{cal}, and values of the measured sound pressure spectrum, SPL_M. The reflectance used to account for the reflection effects is similar to that shown in figure 3(a). Comparison of SPL_{cal} with the measured SPL data, SPL_M, indicates a good representation of the data was achieved.

Figure 13(c) illustrates the fit between PSD_M^+ and PSD_{cal}^+. A good least-squares curve fit was again achieved.

Variations with angle and velocity. - Calculations were also made with the iteration method developed using data from the full-scale engine EBF configuration previously discussed taken at microphone angles from 20° to 140° over a range of exhaust velocities. Figure 14 shows values of $OASPL_p^+$ determined by the curve fitting procedure. The lossless values of OASPL were calculated from the value of lossless SPL. Slopes of $OASPL^+$ following a sixth or an eighth power of the effective velocity are shown in the figure for comparison purposes.

According to figure 14, for microphone angles between 20° and 90° the $OASPL_p^+$ varies with the sixth power of the effective exhaust velocity reflecting the dominance of surface scrubbing (or dipole) noise. For angles between 100° and 140°, the data in figure 14 indicate a trend toward an eighth power dependence on effective velocity. At 120° the eighth power relation fits the data quite well. This is interpreted to be an indication that the jet (or quadruple mixing) noise source is more important at these greater angles.

Figure 15 shows PSD_{cal}^+ for angles from 40° to 120° at the maximum power setitng with $V_e = 242$ m/sec (795 ft/sec). The curves for microphone angles of 40° to 80° (sixth power of velocity region) are similar in appearance and peak at a Strouhal number between 0.25 and 0.27. The PSD_{cal}^+ curves for microphone angles of 100° and 120° (eighth power of velocity region) have their peak values at a Strouhal number between 0.30 and 0.35. All the PSD^+ curves fall within a band of less than 4 dB width.

CONCLUDING REMARKS

A calculation procedure based on a simple rational function for spectral density has been shown to provide a representation for the acoustic spectra generated by deflection of engine exhaust jets for under-the-wing and over-the-wing versions of externally blown flap configura-

tions. The representation is useful in correcting reflection effects, and provides a compact method of storing sound spectral data. In addition, the simple function is related to a more basic pressure spectral density function that can also be used to fit PSD data and can be related to scrubbing noise theory.

The simple rational function combined with the procedure for correcting reflection effects yields mean-square pressure level per unit Strouhal number curves that are devoid of interference effects and can be easily compared with one another.

SYMBOLS

$A_c(\Omega)$	correlation area over which the normalized cross spectral density of the normal stress is unity
$A_T(f_c,r)$	atmospheric attenuation, dB
a_i	zero of $\phi(\Omega)$, i = 1, 2, . . ., M_a
a_o	a complex number, normalization constant
b_k	pole of $\phi(\Omega)$, k = 1, 2, . . ., M_b
C_e	cost function, sum of square of error between measured and calculated sound spectra
C_p	penalty function
C_T	total cost function
C_1,C_2,C_3	cancellation frequencies
c	a complex number
c_o	velocity of sound, m/sec
D_e	effective diameter, m
d_m	a complex constant, m = 1, 2, . . ., K_d
F(c)	Strouhal response function
f	frequency, Hertz
f_c	nominal mean frequency, Hertz
G(s)	reflected ray transfer function
$g(\tau)$	reflecting surfaces' impulse response function

h_o	microphone height, m
$h_s(n)$	height of n^{th} source, m
K_d	number of $\sigma(\Omega,d_m)$ terms in $A_c(\Omega)$ and $\psi(\Omega)$
ℓ	third-octave band number
M_a	number of numerator $\sigma(\Omega,a_i)$ terms of $\phi_{Real}(\Omega)$
N	number of independent noise sources
N_b	number of denominator $\sigma(\Omega,b_k)$ terms of $\phi_{Real}(\Omega)$
n	source index
OASPL	overall sound pressure level relative to p_r, dB
$OASPL_p^+$	lossless OASPL parametric value, dB
PSD	Strouhal normalized mean-square pressure level per unit Strouhal number, dB
PSD^+	PSD without atmospheric absorption and ground reflection effects, dB
PSD_{cal}^+	PSD^+ calculated from formula, dB
PSD_M^+	PSD^+ calculated from measured data, dB
$PSD_{Real}^+(\Omega)$	PSD^+ calculated from a real random process spectrum density, dB
p	pressure, N/m^2
p'	reflected pressure signal, N/m^2
p_r	reference pressure 2×10^{-5} N/m^2 (2×10^{-4} microbar)
$\|Q(s)\|$	magnitude of reflected ray transfer function
R_2,R_3,R_4	reinforcement frequency
r	distance from source to microphone
$S(\vec{x})$	surface immersed in a flow
SPL	third-octave sound pressure level reference to p_r, dB
SPL^+	third-octave sound pressure level referenced to p_r that would be measured without atmospheric attenuation and in the absence of reflecting surface, dB

SPL_{cal}	SPL calculated from an equation, dB
SPL_M	SPL measured, dB
St	Strouhal number, $f(D_e/V_e)$
St_o	constant, Strouhal number (0.3, ref. 14)
s	$j2\pi f$, $j\omega$
s_1	distance from source to microphone along direct ray path, m
s_2	distance from source to microphone along reflected ray path, m
$\lvert T(f_c) \rvert^2$	reflectance
t	time, sec
V_e	effective velocity, m/sec
$\vec{x}$	surface position vector
z	mean ratio of path length reflected ray traveled to path length direct ray traveled for all n sources
α_o	real constant, $-2\pi St_o$
Δf_c	bandwidth at center frequency f_c ($0.2316\ f_c$), hertz
$\delta(s)$	reflected ray transfer function phase factor, rad (deg)
θ	microphone angle relative to inlet
$\sigma(\Omega,c)$	function of Strouhal number such that the reciprocal of the Fourier transform of a "damped oscillation" is proportional to $\lvert \sigma(\Omega,c) \rvert^2$
τ	time delay, sec
τ_n	time delay between arrival of wave leaving source at time t and traveling direct path to receiver and one leaving at time t and traveling reflected ray path to receiver, sec
$\phi(\Omega)$	Strouhal normalized mean-square pressure per unit Strouhal number
$\phi_{Real}(\Omega)$	Strouhal normalized mean-square pressure per unit Strouhal number for a real random process
$\psi(\Omega)$	spectrum of the pseudo-soumd or fluctuating surface pressure

Ω relative angular velocity, $j2\pi f(D_e/V_e) = j2\pi St$

ω angular velocity, $2\pi f$, rad/sec

$\prod_{i=m}^{n}$ product of terms with index i ranging from m to n

$\sum_{i=m}^{n}$ summation, sum of terms of index i ranging from m to n

j $\sqrt{-1}$

Superscript:

$*$ denotes conjugate

REFERENCES

1. Clark, L. T.: The Radiation of Sound from an Airfoil Immersed in a Laminar Flow. Paper 71-GT-4, Mar. 1971, ASME.

2. Dorsch, R. G.; Krejsa, E. A.; and Olsen, W. A.: Blown Flap Noise Research. Paper 71-745, June 1971, AIAA, New York, N.Y.

3. Dorsch, R. G.; Kreim, W. J.; and Olsen, W. A.: Externally Blown Flap Noise. Paper 72-129, Jan. 1972, AIAA, New York, N.Y.

4. Reshotko, M.; Goodykoontz, J. H.; and Dorsch, R. G.: Engine Over-the-Wing Noise Research. Paper 73-631, July 1973, AIAA, New York, N.Y.

5. Dorsch, R. G.; and Reshotko, M.: EBF Noise Tests with Engine Under- and Over-the-Wing Configurations. STOL Technology, SP-320, 1973, NASA, Washington, D.C.

6. Dorsch, R. G.; and Reshotko, M.; and Olsen, W. A.: Flap Noise Measurements for STOL Configurations Using External Upper Surface Blowing. Paper 72-1203, AIAA, Nov.-Dec. 1972.

7. Dorsch, R. G.; Goodykoontz, J. H.; and Sargent, N. B.: Effect of Configuration Variations on Externally Blown Flap Noise. Paper 74-190, AIAA, Jan.-Feb. 1974.

8. Goodykoontz, J. H.; Dorsch, R. G.; and Wagner, J. M.: Acoustic Characteristics of a Mixer Nozzle-EBF System. Paper 74-192, AIAA, Jan.-Feb. 1974.

9. Samanich, N. E.; Heidelberg, L. J.; and Jones, W. L.: Effect of Exhaust Nozzle Configuration on Aerodynamic and Acoustic Performance of an Externally Blown Flap System with a Quiet 6:1 Bypass Ratio Engine. Paper 73-1217, Nov. 1973, AIAA, New York.

10. Jones, W. L.; Heidelberg, L. J.; and Goldman, R. G.: Highly Noise Suppressed Bypass 6 Engine for STOL Applications. Paper 73-1031, Oct. 1973, AIAA, New York, N.Y.

11. Olsen, William A.; Miles, Jeffrey H.; and Dorsch, Robert G.: Noise Generated by Impingement of a Jet upon a Large Flat Board. NASA TN D-7075, Dec. 1972.

12. Olsen, W. A.; Dorsch, R. G.; and Miles, J. H.: Noise Produced by a Small Scale Externally Blown Flap. NASA TN D-6636, 1972.

13. Hayden, R. E.: Noise from Interaction of Flow with Rigid Surfaces: A Review of Current Status of Prediction Techniques. NASA CR-2126, Oct. 1972.

14. Fink, Martin R.: Mechanisms of Externally Blown Flap Noise. Paper 73-1029, Oct. 1973, AIAA, New York, N.Y.

15. Clark, B. J.; Dorsch, R. G.; and Reshotko, M.: Flap Noise Prediction Method for a Powered Lift System. Paper 73-1028, Oct. 1973, AIAA, New York, N.Y.

16. Curle, N.: The Influence of Solid Boundaries Upon Aerodynamic Sound. Proc. Roy. Soc., A, 231, 505, 1955.

17. Kraichnan, R. H.: Pressure Fluctuations in Turbulent Flow Over a Flat Plate. J. Acoust. Soc. Am., vol. 28 (3), May 1956.

18. Phillips, O. M.: On the Aerodynamic Surface Sound from a Plane Turbulent Boundary Layer. Proc. Roy. Soc. Am, A234, pp. 327-335 (1956).

19. Powell, Alan: Aerodynamic Noise and the Plane Boundary. J. Acoust. Soc. Am., 32, 982, 1960.

20. Meecham, W. C.: Surface and Volume Sound from Boundary Layers. J. Acoust. Soc. Am., 37, 516, 1965.

21. Clark, P. J. F. and Ribner, H. S.: Direct Correlation of Fluctuating Lift with Radiated Sound for an Airfoil in Turbulent Flow. J. Acoust. Soc. Am., vol. 46 (3), 1969.

22. Siddon, Thomas E.: Surface Dipole Strength by Cross-Correlation Method. J. Acoust. Soc. Am., vol. 53 (2), 1973.

23. Hersh, A. S.; and Meecham, W. C.: Sound Directivity Pattern Radiated by Small Airfoils. J. Acoust. Soc. Am., vol. 53 (2), 1973.

24. Sharland, I. J.: Sources of Noise in Axial Flow Fans. J. Sound Vib. (1964), I (3), pp. 302-322.

25. Vecchio, E. A.; and Wiley, C. A.: Noise Radiated from a Turbulent Boundary Layer. J. Acoust. Soc. Am., vol. 53 (2), 1973.

26. Thomas, P.: Etude des Interferences Acoustiques Par Reflexion Application Aux Spectres de Pression Acoustique des Jets. AGARD CP42 (St. Louis; Mar. 1969).

27. Mariano, Sulmo, et al.: Ground Effect of a Plane Uniform Sound Source Distribution. Boeing D6-22600 TN, 1/20/69, N70-19730.

28. Howes, W. L.: Ground Reflection of Jet Noise. NASA TR-35 (1959).

29. Franken, P. A.: A Theoretical Analyses of the Field of a Random Noise Source Above an Infinite Plane. NACA TN-3557, 1955.

30. Hoch, R.; and Thomas, P.: Influence des reflexions sur les spectres de pression acoustique des jets. Premier Collogue d'Acoustique (Toulouse, 1968).

31. Morse, P. M.; and Ingard, K. V.: Theoretical Acoustics. McGraw-Hill Book Co., 1968.

32. Evans, L. B.; and Sutherland, L. C.: Wyle Labs. Res. Staff, WR 70-14, 1970.

33. Aoki, Masano: Introduction to Optimization Techniques. The MacMillan Co., 1971.

34. Pierre, D. A.: Optimization Theory with Applications. John Wiley & Sons, Inc., 1969.

35. Powell, M. J. D.: An Efficient Method for Finding the Minimum of a Function of Several Variables Without Calculating Derivatives. Computer Journal, vol. 7, 1964, pp. 155-162.

36. Shapero, M. S.; and Goldstein, M.: A Collection of Mathematical Computer Routines. AEC-NYO-1480, 14, Feb. 1965, New York University, New York, N.Y.

37. Miles, J. H.: Computer Method for Identification of Boiler Transfer Functions. NASA TM X-2436, 1971.

TABLE I. - CONSTANTS USED IN REFLECTANCE CALCULATIONS

(a) Constants used for reflectance shown in figure 2. N = 5; r = 15.24 m (50 ft); h_m = 3.88 m (12.75 ft)

n		1	2	3	4	5
$h_s(n)$	m	4.130	4.0081	3.886	3.764	3.642
	ft	13.55	13.15	12.75	12.35	11.95
τ_n	sec	0.0058	0.00567	0.0055	0.0053	0.0052

(b) Constants sued for reflectance shown in figure 3. N = 5; r = 30.48 m (100 ft); h_m = 12.743 m (9 ft)

n		1	2	3	4	5
$h_s(n)$	m	3.475	3.736	2.743	2.377	2.012
	ft	11.4	10.2	9.0	7.8	6.6
τ_n	sec	0.00182	0.00164	0.00145	0.00125	0.00106

TABLE II. - PARAMETERS TO CALCULATE SELECTED PSD^{+}_{Real} CURVES USING EQUATIONS (6) AND (4b)

Dimensionless parameter	Complex number, C (real value, imaginary value), C = a_0, a_1, b_1, b_2, or b_3			
	Data of fig. 5	Data of fig. 6	Data of fig. 7(a)	Data of fig. 7(b)
a_0	(151.610, 151.610)	(133.3510, 133.3510)	(372.2495, 372.2495)	(293.9065, 293.9065)
a_1	(-0.1965826, 0.1824718)	(-0.1304851, 0.1214311)	(-0.7096163, 0.6316123)	(-0.4733036, 0.2092519)
b_1	(76.22998, 26.7030)	(-0.1540204, 0.4026451)	(-0.3045551, 1.036240)	(-0.4142318, 0.7848299)
b_2	(-0.9577132, 0.7647091)	(-1.564607, 1.282075)	(-3.892744, 3.885970)	(-4.280862, 3.136002)
b_3	(-1.546595, 2.192013)	(-76.433486, 35.98859)	(-156.9277, 15.68585)	(-87.00853, 66.38647)

TABLE III. - PARAMETERS TO CALCULATE SELECTED PSD^{+}_{Cal} CURVES USING EQUATION (10)

Dimensionless parameter	Complex number, C (real value, imaginary value), C = a_0, a_1, b_1, b_2, or b_3			
	Data of fig. 5	Data of fig. 6	Data of fig. 7(a)	Data of fig. 7(b)
a_0	(192.6902, 192.6902)	(105.7856, 105.7856)	(290.5190, 290.5198)	(268.0784, 268.0784)
a_1	(-0.2528992, 0.1505393)	(-0.1947860,0.06866252)	(-0.1126150,0.08250151)	(-0.1289076, 0.0709157)
b_1	(-1.194895, 0.5249010)	(-0.1479430, 0.4224659)	(-0.4334988, 0.3890225)	(-0.4899988, 0.424448)
b_2	(-1.745644, 1.715307)	(-1.963396, 1.474141)	(-3.177522, 0.5692431)	(-3.651598, 0.3990379)
b_3	(-115.7714, 14.24272)	(-73.48344, 45.69005)	(-124.6561, 34.93369)	(-98.45943, 52.17599)

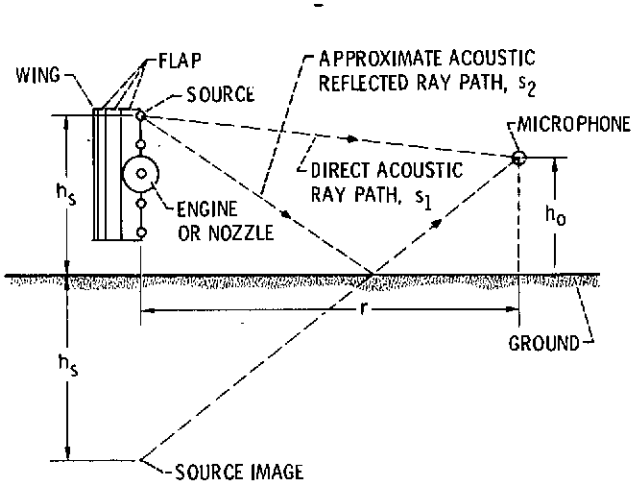

Figure 1. - Schematic of source and microphone geometry relative to ground.

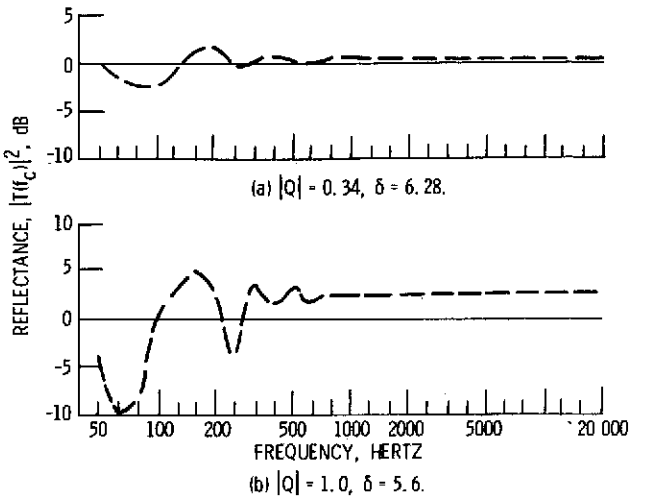

Figure 2. - Calculated reflectance (eq. (14)) for test site used to obtain cold flow blown flap data in reference 4 evaluated for a low and high level of |Q|.

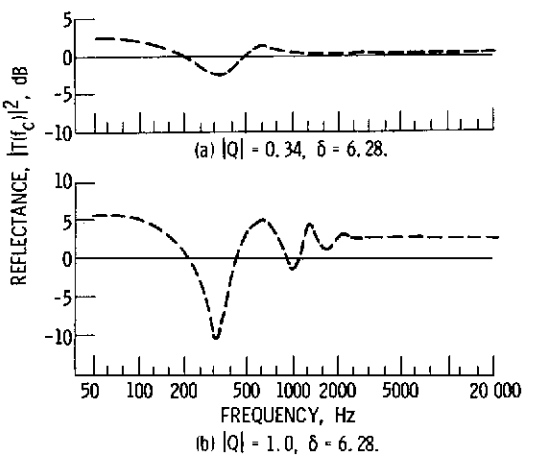

Figure 3. - Calculated reflectance (eq. (14)) for test site used to obtain turbofan engine externally-blown-flap data (ref. 9) evaluated for a low and high level of |Q|.

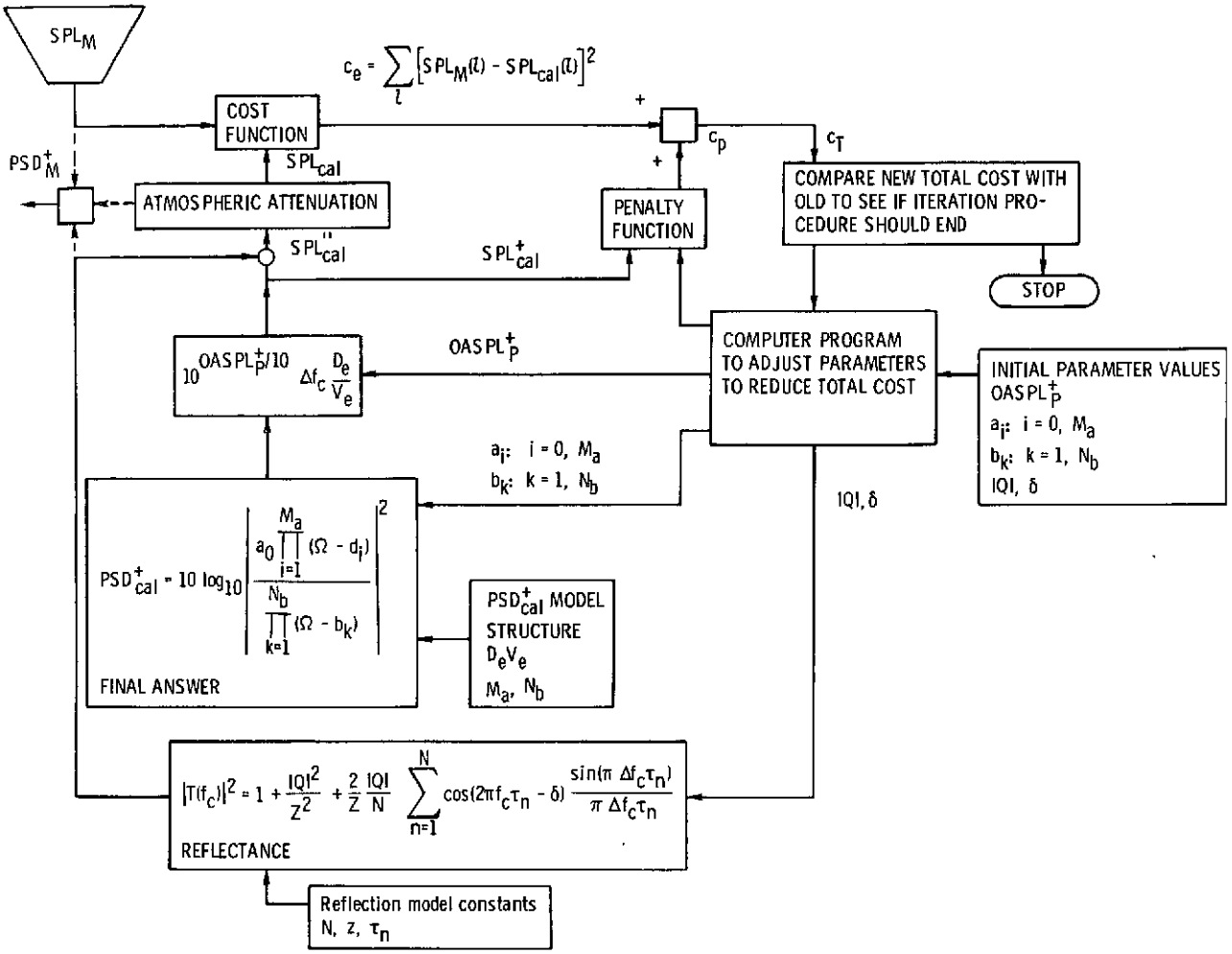

Figure 4. - Diagram of computer method.

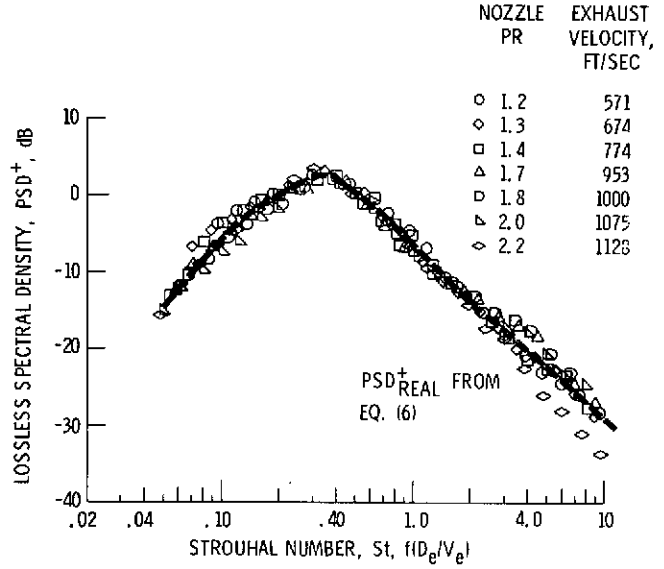

Figure 5. - Comparison of curve fit using equation (6) with Strouhal correlation of cold flow under-the-wing externally-flap data taken from reference 3. Flap setting, 30^0 - 60^0; microphone angle, 85^0.

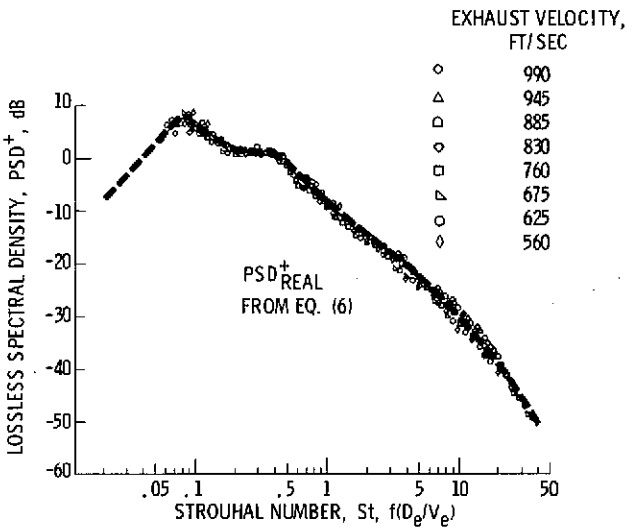

Figure 6. - Comparison of curve fit using equation (6) with Strouhal correlation of data for engine-over-the-wing externally-blown-flap configuration with powered lift taken from reference 4. Flap setting 10^0 - 20^0; microphone angle, 100^0.

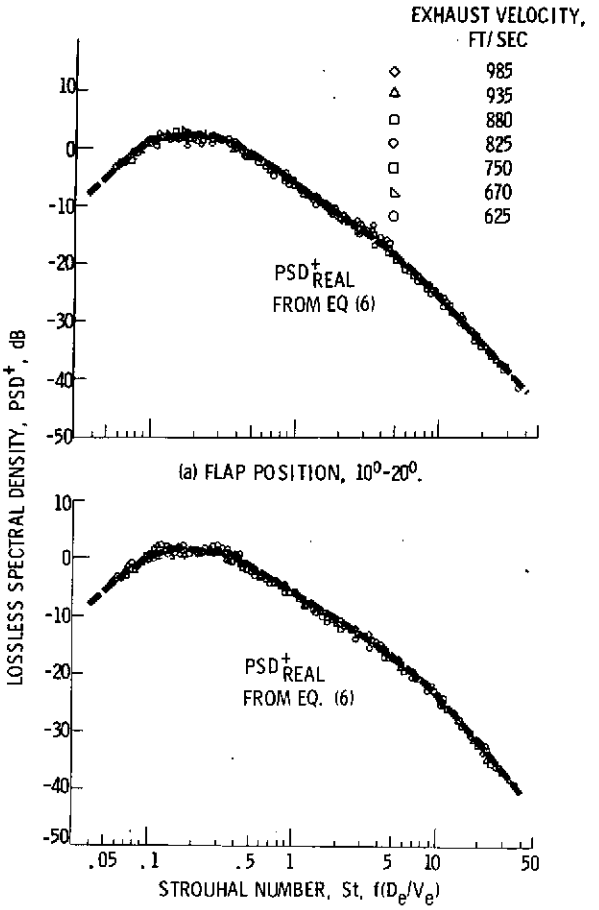

Figure 7. - Comparison of curve fit using equation (6) with Strouhal correlation of data for the engine-over-the wing externally-blown-flap configuration with conventional lift taken from reference 4. Microphone angle, 120^0.

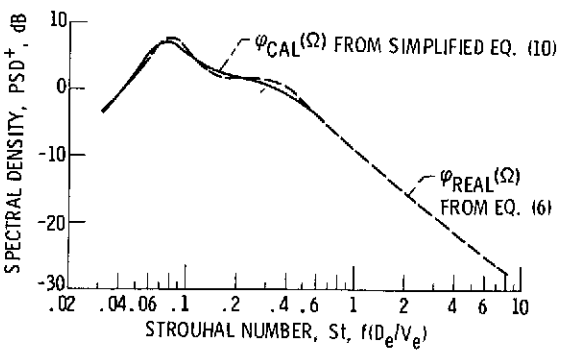

Figure 8. - Comparison of use of basic and simplified spectral density functions to fit data of figure 6.

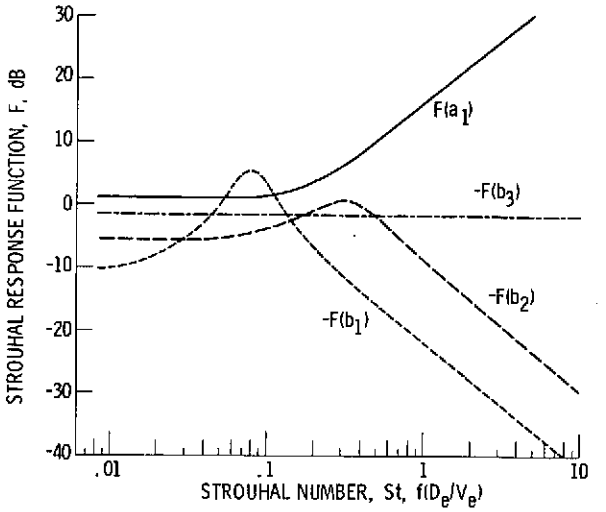

Figure 9. - Strouhal response functions used to produce simplified PSD^+ function in figure 8.

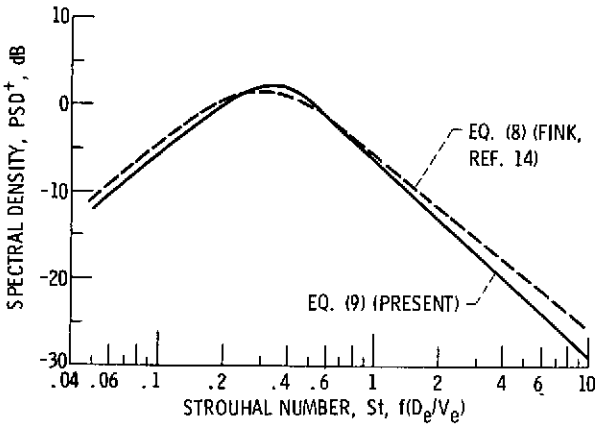

Figure 10. - Plot of PSD^+ functions based on data shown in figure 5. Comparison is made between three parameter curve fit based on equation (8) and seven parameter curve fit based on equation (9).

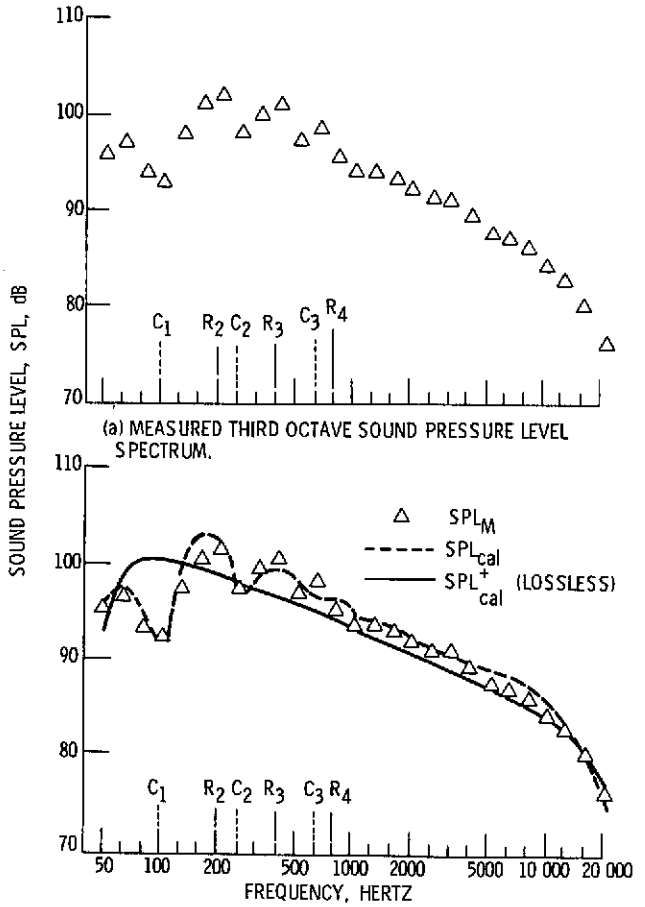

Figure 11. - Over-the-wing cold-flow powered lift model with flap position 10^0 - 20^0 (ref. 4). Exhaust velocity, 253 m/sec (830 ft/sec); distance, 15.2 m (50 ft). Microphone height, 3.9 m (12.75 ft); source height, 3.9 m (12.75 ft); microphone angle, 100^0.

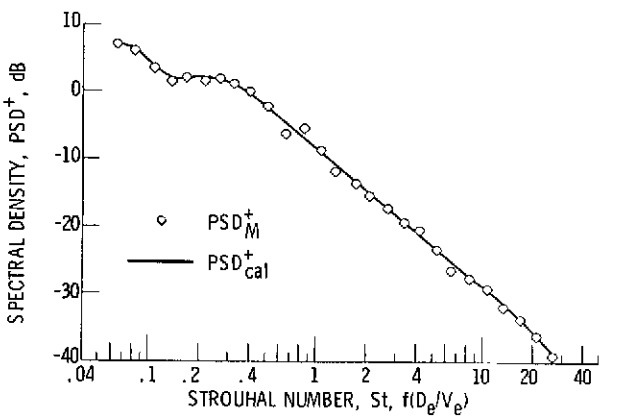

Figure 12. - Comparison of measured and calculated spectral density using over-the-wing cold-flow powered lift model data of figure 11. V_e = 253 m/sec (830 ft/sec).

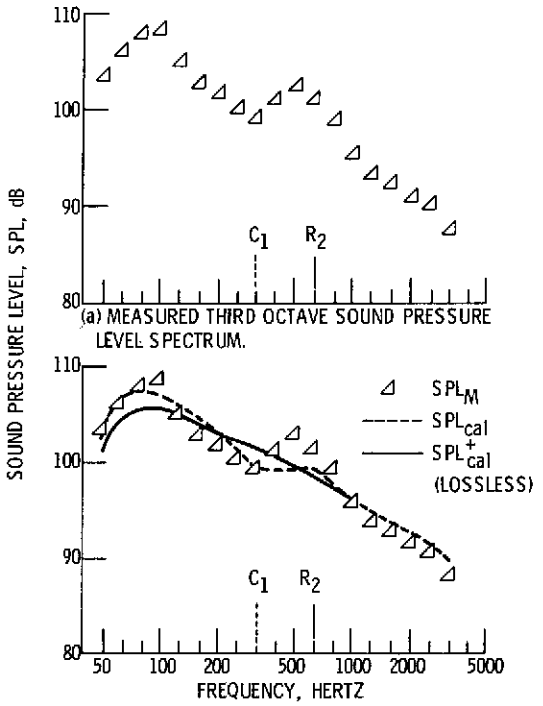

(a) MEASURED THIRD OCTAVE SOUND PRESSURE LEVEL SPECTRUM.

(b) MEASURED AND CALCULATED SOUND PRESSURE LEVEL SPECTRUM.

Figure 13. - Turbofan engine externally-blown-flap configuration with effective exhaust velocity, 242.3 m/sec (795 ft/sec); distance, 30.48 m (100 ft); microphone and source height, 2.74 m (9 ft); microphone angle, 80^0.

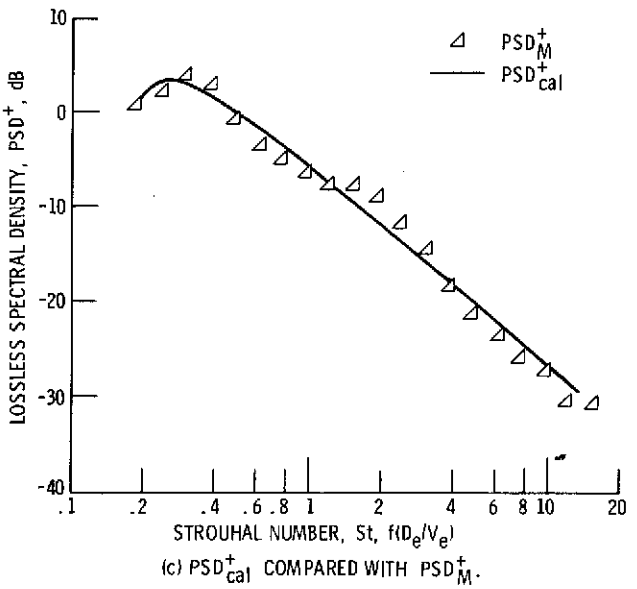

(c) PSD^+_{cal} COMPARED WITH PSD^+_M.

Figure 13. - Concluded.

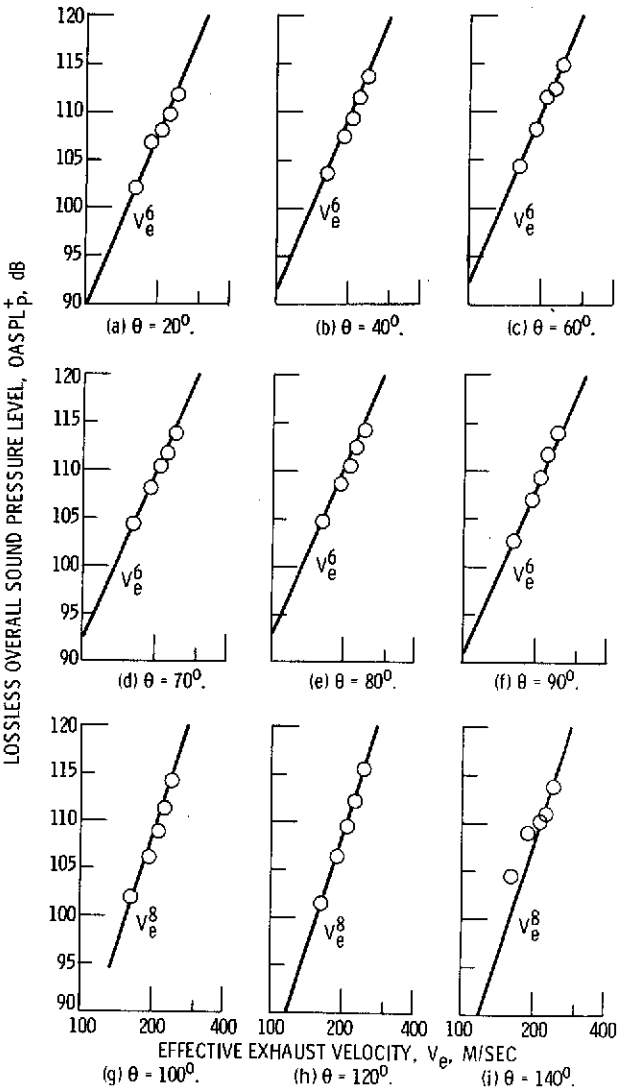

Figure 14. - Variation of lossless overall sound pressure level with effective velocity at microphone angles, θ, from 20^0 to 140^0 for turbofan engine EBF configurations. Flap setting, 0^0-20^0-40^0. Microphone radius, 30.48 m (100 ft).

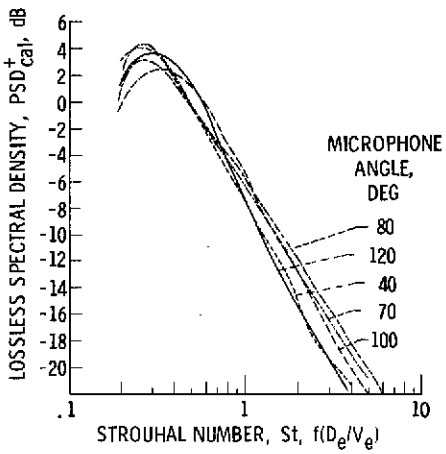

Figure 15. - Variation of calculated lossless spectral density PSD^{+}_{cal} at effective exhaust velocity of 242.3 m/sec (795 ft/sec) with microphone position over a range of angles from 40^0 to 120^0. Turbofan engine EBF configuration, flap setting, 0^0-20^0-40^0.